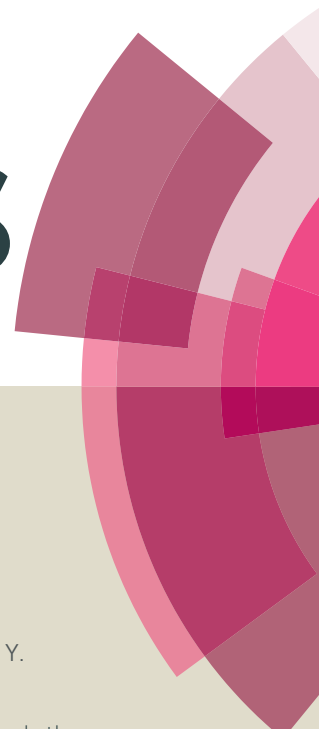


# RSC Advances



This article can be cited before page numbers have been issued, to do this please use: S. Chi, L. Li and Y. Wu, *RSC Adv.*, 2016, DOI: 10.1039/C6RA12193D.



This is an *Accepted Manuscript*, which has been through the Royal Society of Chemistry peer review process and has been accepted for publication.

*Accepted Manuscripts* are published online shortly after acceptance, before technical editing, formatting and proof reading. Using this free service, authors can make their results available to the community, in citable form, before we publish the edited article. This *Accepted Manuscript* will be replaced by the edited, formatted and paginated article as soon as this is available.

You can find more information about *Accepted Manuscripts* in the [Information for Authors](#).

Please note that technical editing may introduce minor changes to the text and/or graphics, which may alter content. The journal's standard [Terms & Conditions](#) and the [Ethical guidelines](#) still apply. In no event shall the Royal Society of Chemistry be held responsible for any errors or omissions in this *Accepted Manuscript* or any consequences arising from the use of any information it contains.

# Novel mono-cationic fluorescent probes based on different central $\pi$ -conjugated bridges for two-photon bioimaging of cellular nucleus

Shuheng Chi<sup>a,b</sup>, Liang Li<sup>a,b</sup>, Yiqun Wu<sup>a,c,\*</sup>

<sup>a</sup> Key Laboratory of Material Science and Technology for High Power Lasers, Shanghai Institute of Optics and Fine Mechanics, Chinese Academy of Sciences, Shanghai 201800, PR China

<sup>b</sup> University of Chinese Academy of Sciences, Beijing 100049, PR China

<sup>c</sup> Key Lab of Functional Inorganic Material Chemistry (Heilongjiang University), Ministry of Education, Harbin 150080, PR China

\*Corresponding author. Tel.: +86 021 6991 8592

Email Address: \*yqwu@siom.ac.cn

## Abstract

A series of novel pyridine mono-cationic two-photon fluorescent probes based on different central  $\pi$ -conjugated bridges, fluorenone (W-pyI), dibenzothiophene (S-pyI), and dibenzofuran (F-pyI), were prepared and studied. Under one-photon excitation in N,N-dimethylformamide solution, W-pyI, S-pyI, and F-pyI displayed fluorescence quantum yields of 0.401, 0.425, and 0.09, respectively. The two-photon fluorescence performance indicated that these probes possessed two-photon absorption cross-sections of 681 GM (W-pyI), 630 GM (S-pyI), and 620 GM (F-pyI) at 800-nm femtosecond laser excitation. The luminance “turn-on” effect of W-pyI, S-pyI, and F-pyI bonding with calf thymus DNA in Tris-HCl buffer solutions displayed 58-fold, 30-fold, and 25-fold fluorescence quantum yield increments, respectively, and 350–450% two-photon absorption cross-section enhancement. The confocal fluorescence imaging showed clear one- and two-photon fluorescence imaging. The mean co-localization coefficients between these probes and Hoechst 33342 in 3T3 cells ranged from 0.89–0.92, indicating that they showed excellent nuclear targeting abilities. The counterstaining experiments exhibited these probes possessed good counterstaining compatibility and membrane permeability in the application of multicolor targeting. The time-dependent fluorescence intensity test under continuous femtosecond laser irradiation showed that W-pyI possessed a longer observation time (3000 seconds) and a lower fluorescence attenuation amplitude (7.1%) in the first 300

seconds than S-pyI, F-pyI and other previously reported pyridinium derivatives, demonstrating that the central  $\pi$ -conjugated bridge “fluorenone” played a key role in improving photostability during probe designing for two-photon bioimaging applications.

## Introduction

Confocal fluorescence microscopy has become a powerful tool for the observation of cells, tissues, and vital organs. Compared with traditional biological optical microscopy, two-photon fluorescence microscopy provides a key technique for tracking and monitoring of living cells because it employs a near-infrared excitation light source, and provides a low damage threshold, a high penetration depth, and high-resolution three-dimensional space selectivity [1-4]. However, two-photon fluorescent probes remain an issue of widespread concern. Numerous reports have been published on selective labeling of mitochondria, lysosomes, metal ions, and other living tissues [5-9]; however, most of the probes show poor lipophilicity and hydrophilicity, low photostability, and high toxicity. In addition, few studies have been published on the effectiveness of nuclear localization using different  $\pi$ -conjugated structural fluorescent probe molecules in two-photon fluorescence imaging. In particular, photostability under continuous femtosecond laser irradiation during real-time monitoring and tracking of cellular nuclei in living cells has rarely been reported. This issue needs to be further investigated.

Recently, some two-photon fluorescent probes with good performance were prepared for two-photon bioimaging in cellular or subcellular levels. Zheng et al. [10] designed a novel two-photon fluorescent cyanine, whose two-photon absorption (TPA) cross-section in glycol reached 497 GM, and the 30-fold one-photon fluorescence enhancement and 3-fold enhancement of TPA cross-section were achieved when binding with calf thymus DNA in buffer solutions. Miao et al. [11] prepared two pyridine cation derivatives for specific mitochondrial imaging. The maximum TPA action cross-section at 860 nm reached 328 GM, and the fluorescence attenuation amplitude was 10% and 20% within 300 s, respectively. Liu et al. [12] designed two indole-based mono-cationic probes for selective imaging of cellular RNA in nucleoli and cytoplasm. The TPA action cross-section of INR1 at 800 nm in the presence of DNA and RNA in buffer solutions was 5.71 and 8.93 GM, respectively. The fluorescence signals of INR1 and INR2 decreased by 8% and 28% after 300 s of irradiation. Wang et al. [13] prepared a two-photon ratiometric fluorescent pH probe, whose TPA cross-section was 354 GM at pH 4.5 with good membrane permeability. Xu et al. [14] also reported a novel series of dinuclear Ru(II) polypyridyl complexes

for cellular cytoplasm imaging, whose maximum TPA cross-sections were estimated to be 322–386 GM, and the fluorescence signals of RuL<sub>4</sub> decreased by 38% within 300 s under laser irradiation. The distribution percentage of the probe in the cytoplasmic region reached 90%.

An excellent two-photon nuclear fluorescent probe should not only have a sufficiently large two-photon absorption cross-section, but also possess strong nuclear DNA-targeting ability. A probe with these two properties would exhibit good photostability characteristics for nuclear monitoring and imaging. Therefore, the structure-property relationship has always been the focus of attention in the design of molecular structures [15-17]. According to several previous reports, two-photon fluorescent probes with large TPA cross-sections must have the following structural characteristics: high acceptor and donor strength, a long molecular chain, good conjugated delocalized planarity, and structural symmetry [18-22]. However, to possess sufficient affinity to nuclear DNA in the complex cellular microenvironment, the probes must possess some additional important structural features [23-25]: first, molecules should have a donor-acceptor-donor type system for efficient charge transfer in the sensitive bioenvironment; second, V-shaped aryl arms that cause fluorescence enhancement and the “turn-on” effect by restricting planar rotation; third, the terminal units in the molecular structure should have the ability to recognize DNA base pairs by electrostatic attraction, and the central  $\pi$ -conjugated bridge should become embedded into the phosphate backbone of double-stranded DNA through groove binding or intercalative binding. Based on the above theoretical guidelines, we designed three symmetric V-shaped two-photon fluorescent probes with pyridine mono-cationic units and different central  $\pi$ -conjugated bridges (fluorenone, dibenzothiophene, and dibenzofuran), referred to as W-pyI, S-pyI, and F-pyI (Scheme 1). The “dibenzothiophene” conjugated core had been used to connect with symmetric pyridine rings in our previous study. To facilitate comparison of two-photon performance, molecules with “fluorenone” and “dibenzofuran” aromatic cores were prepared, to investigate the influences of different center conjugated bridges on the structure-property relationships and biological fluorescence imaging performance. Here, the one- and two-photon photophysical properties of W-pyI, S-pyI, and F-pyI were studied, including calculation and analysis of TPA cross-sections upon excitation using a 750–830 nm femtosecond laser source and fluorescence quantum yields in N,N-dimethylformamide (DMF) solution. The ct-DNA fluorescence switching characteristics in tris(hydroxymethyl) methyl aminomethane-chlorine hydride (Tris-HCl) buffer solutions were researched, and the influences of the various conjugated aromatic cores on fluorescence “turn-on” effect bounding with DNA were also investigated. The one- and two-photon confocal fluorescence imaging at the

excitation wavelength of 405 nm and 800 nm in 3T3 cells were carried out. Nuclear co-localization staining experiments were conducted between W-pyI, S-pyI, or F-pyI and Hoechst 33342 (a commercial nuclear staining reagent). The counterstaining experiment employing W-pyI, S-pyI or F-pyI double-stained with MitoTracker Red CMXRos (MTR, a commercial red mitochondrial staining reagent) were performed as well. The variations in fluorescence intensity with time under continuous 800-nm femtosecond laser irradiation in the process of two-photon nuclear imaging were studied, along with the effects of the three different central  $\pi$ -conjugated bridges on photostability.

## Experimental section

### Materials

All solvents and reagents were of analytical grade and were purchased from Sinopharm Chemical Reagent Co., Ltd. (Shanghai, China). 2,7-Dibromo-9-fluorenone, 2,8-dibromodibenzothiophene, and 2,8-dibromodibenzofuran were purchased from Alfacem Co. (Zhengzhou, China). Methyl iodide ( $\text{CH}_3\text{I}$ ) and Tris(hydroxymethyl) methyl aminomethane (Tris) were obtained from J&K Chemical (Beijing, China). 4-Vinylpyridine, MitoTracker Red CMXRos (MTR), Hoechst 33342, and calf thymus DNA (ct-DNA) were obtained from Thermo Fisher Scientific (Waltham, USA). Samples and ct-DNA dissolved in Tris-HCl buffer solution (Tris: 10 mM, NaCl: 100 mM, pH = 7.4) were prepared at concentrations of  $10^{-5}$  M and  $0\text{--}1.4 \times 10^{-3}$  M, respectively. All chemicals were stored at 4 °C until use.

### Synthesis of W-pyI/S-pyI/F-pyI

The synthesis process was divided into two steps. First, 2,7-dibromo-9-fluorenone (4.05 g, 0.012 mol), 2,8-dibromodibenzothiophene (4.10 g, 0.012 mol), or 2,8-dibromodibenzofuran (4.21 g, 0.013 mol), 4-vinylpyridine (0.50 g, 0.048 mmol), tri(o-tolyl)phosphine (0.46 g, 1.50 mmol), palladium (II) acetate (0.03 g, 0.13 mmol), triethylamine (20 ml, 0.14 mol), and 15 ml DMF were added and mixed uniformly in a closed reaction vessel, which was filled with high-purity nitrogen at a pressure of 3 MPa. Under the protection of the inert gas, the temperature gradually rose to 110 °C, thermal insulation 24 h. After the reaction, the mixed liquid was fully extracted with dichloromethane, and the crude product was obtained by vacuum distillation. Then a red intermediate product (W-py, S-py, or F-py) was separated out via column chromatography using ethyl acetate-petroleum (4:1) and acetonitrile-dichloromethane (3:1) on silica gel; second, the intermediate product W-py (3.475 g, 0.009 mol), S-py (3.901 g, 0.010 mol) or F-py (3.367 g, 0.009 mol), methyl iodide (2.129 g, 0.015 mol) and 40 ml of acetone were added in turn to a round-bottomed flask, then the temperature was gradually increased to 85 °C for 18 h. After cooling, an orange-red (W-pyI) or pale yellow (S-pyI, F-pyI) target product was separated out via vacuum

distillation and column chromatography.

**W-pyI:** Yield: 3.85 g (80 %). Mp > 290 °C. <sup>1</sup>H NMR (DMSO, 500 MHz): δ 8.90 (d, 4H), 8.82 (d, 1H), 8.23 (d, 4H), 8.12 (d, 1H), 7.98 (m, 8H), 4.27 (s, 3H). <sup>13</sup>C NMR (DMSO, 125 MHz): δ 194.14, 154.27, 147.38, 146.65, 141.23, 139.12, 137.80, 136.77, 126.66, 125.88, 125.18, 124.83, 124.53, 49.25. MALDI-TOF-MS: m/z calcd [M-I]<sup>+</sup> for C<sub>28</sub>H<sub>21</sub>IN<sub>2</sub>O, 401.172; found, 401.251. Anal. calcd. for C<sub>28</sub>H<sub>21</sub>IN<sub>2</sub>O (%): C 63.65, H 4.01, N 5.30, O 3.03; found: C 63.83, H 4.71, N 5.22, O 3.19.

**S-pyI:** Yield: 3.69 g (76 %). Mp > 290 °C. <sup>1</sup>H NMR (DMSO, 400 MHz): δ 8.93 (d, 2H), 8.88 (m, 2H), 8.27 (t, 2H), 8.25 (m, 2H), 8.20 (d, 2H), 7.98 (m, 2H), 7.96 (m, 2H), 7.83 (s, 2H), 7.79 (t, 2H), 4.28 (m, 3H). <sup>13</sup>C NMR (DMSO, 125 MHz): δ 153.41, 146.28, 141.92, 139.89, 135.34, 133.91, 128.02, 123.92, 122.83, 121.45, 46.88. MALDI-TOF-MS: m/z calcd [M-I]<sup>+</sup> for C<sub>27</sub>H<sub>21</sub>IN<sub>2</sub>S, 405.143; found, 405.137. Anal. calcd. for C<sub>27</sub>H<sub>21</sub>IN<sub>2</sub>S (%): C 60.91, H 3.98, N 5.26, S 6.02; found: C 60.88, H 4.56, N 5.63, S 5.88.

**F-pyI:** Yield: 3.58 g (71 %). Mp > 290 °C. <sup>1</sup>H NMR (DMSO, 500 MHz): δ 8.90 (d, 4H), 8.60 (s, 2H), 8.25 (d, 4H), 8.16 (m, 2H), 7.92 (d, 2H), 7.79 (d, 2H), 7.58 (m, 2H), 4.30 (s, 3H). <sup>13</sup>C NMR (DMSO, 125 MHz): δ 156.88, 152.32, 144.92, 140.26, 130.88, 128.50, 123.83, 123.32, 122.59, 121.02, 112.45, 46.91. MALDI-TOF-MS: m/z calcd [M-I]<sup>+</sup> for C<sub>27</sub>H<sub>21</sub>IN<sub>2</sub>O, 389.176; found, 389.263. Anal. calcd. for C<sub>27</sub>H<sub>21</sub>IN<sub>2</sub>O (%): C 62.80, H 4.10, N 5.43, O 3.10; found: C 63.41, H 4.85, N 5.76, O 2.89.

### Measurements

The absorption spectra were measured using a spectrophotometer (UH-5300, Hitachi, Japan). The one-photon excited fluorescence spectra were obtained using a spectrofluorometer (FP-6500, Jasco, Japan). Rhodamine B in ethanol solution at 25 °C was used as a standard to measure the fluorescence quantum yield. The concentration of the samples and standards used for measuring absorption and one-photon fluorescence spectra was 10<sup>-5</sup> M. The fluorescence quantum yield can be calculated using Eq.(1):

$$\Phi_s = \Phi_r \times \frac{\int F_s}{\int F_r} \times \frac{A_r}{A_s} \times \frac{n_s^2}{n_r^2} \quad (1)$$

The two-photon fluorescence spectra were recorded using a spectrometer (71SW301, Sofn Instruments, China), and excited using a mode-locked Ti:sapphire femtosecond laser system at a pulse duration of 80 fs, with a repetition rate of 80 MHz. Two-photon absorption cross-sections were calculated using the two-photon induced fluorescence method, and Rhodamine B in ethanol solution with a known value was used as the standard at a concentration of 10<sup>-4</sup> M [26,27]. The samples were dissolved in the DMF solvent at a concentration of 10<sup>-4</sup> M. The TPA cross-sections

were determined using Eq.(2):

$$\sigma_s = \sigma_r \times \frac{F_s}{F_r} \times \frac{\Phi_r}{\Phi_s} \times \frac{C_r}{C_s} \times \frac{n_r}{n_s} \quad (2)$$

where the subscripts *s* and *r* represent the sample and standard, respectively.  $\sigma$  is the TPA cross-section, *F* is the two-photon fluorescence integrated area, and *c* and *n* are the concentration and refractive index of the solutions.

### Cellular staining

3T3 mouse myoblasts (0.2  $\mu$ l) were grown in Dulbecco's Modified Eagle Medium (DMEM) containing culture solution under 5% CO<sub>2</sub> at 37 °C for 24 h. After the cells were cultured, they were stained with W-pyI, S-pyI, or F-pyI at concentrations of 0.3  $\mu$ M for 15 min. When completing the staining process, the cover-slips were taken out and inverted on glass slides, which were sealed surrounded by glycerol/water (9:1) solution and preserved by ventilation in the dark.

### Confocal fluorescence imaging

The confocal fluorescence imaging was conducted using a Carl Zeiss LSM 710 confocal scanning microscope. For W-pyI, S-pyI and F-pyI, the one-photon excitation wavelengths were set to 405 nm, and two-photon fluorescence for all samples was excited using an 800-nm femtosecond laser source; the corresponding emission fluorescence was collected in an optical window of 525–575 nm (W-pyI and S-pyI) and 430–490 nm (F-pyI). For Hoechst 33342, the one-photon excitation wavelength was located in the range of 330–380 nm, and the two-photon imaging was excited by a femtosecond laser at 740 nm; the corresponding emission fluorescence was collected in an optical window of 430–490 nm. For MTR, the excitation wavelength was 575 nm, and the emission fluorescence was recorded in the range of 580–650 nm.

## Results and discussion

### One-photon photophysical properties

The absorption spectra of W-pyI, S-pyI, and F-pyI in DMF are shown in Fig.1. The absorption bands of W-pyI and S-pyI were in the range of 375–410 nm and 355–415 nm, respectively, with major absorption peaks at approximately 392 nm and 397 nm. That of F-pyI was between 350–390 nm, with major absorption peaks at approximately 375 nm. Compared with F-pyI, the major absorption peaks of W-pyI and S-pyI were red shifted by ~20 nm, which could be attributed to the relatively larger intramolecular  $n-\pi^*$  transition of W-pyI and S-pyI, due to their functional

“fluorenone” and “dibenzothiophene” aromatic cores [28]. Notably, no absorption was observed between 500–900 nm for any of the materials, indicating that this range could be used as a two-photon excitation window to study their two-photon photophysical properties.

The one-photon fluorescence spectra in DMF are shown in Fig.2. The main fluorescence emission peaks of W-pyI and S-pyI were observed at 540–545 nm, while that of F-pyI was at 480 nm. The Stokes shifts of W-pyI and S-pyI were observed at ~148 nm, higher than that of F-pyI (~105 nm). Under the action of a central electron acceptor, either “fluorenone” or “dibenzothiophene,” the intramolecular charge transfer (ICT) efficiency increased, thus leading to a more stable first excited state that existed in the solvent medium [29]. The fluorescence quantum yields of W-pyI, S-pyI, and F-pyI in DMF were 0.401, 0.425, and 0.09, respectively. Moreover, based on a previous report [30], we also knew that the fluorescence quantum yield of the carbazole dicationic derivative (9E-BMVC) with symmetric pyridine rings in DMF was 0.016. The one-photon photophysical performance data for W-pyI and S-pyI were approximately 4.5-fold and 25-fold, respectively, higher than those of F-pyI and 9E-BMVC, which indicated that with the same mono-cationic pyridine groups, the electron-withdrawing capacity of a “fluorenone” or a “dibenzothiophene” central core is better than that of “dibenzofuran” or “carbazole” in  $\pi$ -conjugated delocalized molecule systems.

### Two-photon photophysical properties

In order to select the optimal two-photon excitation wavelength, the TPA cross-sections of W-pyI, S-pyI, and F-pyI generated by femtosecond laser excitation at 750–830 nm in DMF were calculated, as shown in Fig.3. It could be clearly seen that the TPA cross-sections of W-pyI, S-pyI, and F-pyI were largest (estimated at 681 GM, 630 GM, and 620 GM, respectively) at the wavelengths of 800 nm, 800 nm, and 790 nm, respectively. The TPA cross-sections of F-pyI at 800 nm and 790 nm were nearly identical: 616 GM and 620 GM. Thus, to facilitate comparison, a wavelength of 800 nm was selected as the unified two-photon excitation window to study the two-photon photophysical properties of W-pyI, S-pyI, and F-pyI, especially the influence of the three different central  $\pi$ -conjugated bridges on TPA performance.

The two-photon fluorescence spectra in DMF generated by femtosecond laser excitation at 800 nm are shown in Fig.4. Using the two-photon induced fluorescence method, the TPA cross-sections ( $\sigma$ ) of W-pyI, S-pyI, and F-pyI were estimated to be 681 GM, 630 GM, and 616 GM, respectively while the action TPA cross-sections ( $\sigma \times \Phi$ ) of the probes were approximately 273 GM, 267 GM, and 55 GM, respectively. The two-photon photophysical performance of the previously reported

carbazole-based dicationic salt was studied as well, and showed a  $\sigma$  and  $(\sigma \times \Phi)$  of approximately 360 GM and 5.7 GM, respectively, at 800 nm [30]. Moreover, compared with other recently reported two-photon fluorescent probes, for example, biscarbazolymethane-based cyanine [10],  $\sigma = 497$  GM; ratiometric pH probes [13, 31],  $\sigma = 354$  GM and 142 GM; fluorene derivatives [32],  $\sigma = 400$  GM; DAPI [14],  $\sigma = 0.16$  GM, our new probes showed relatively higher TPA properties. Thus, as all of the above materials had V-shaped symmetric structures, the same molecular chain lengths, and pyridinium salt electron-donating arms, the central conjugate bridge plays a key role in TPA performance. Notably, there are differences in the linkage position of central core and two vinyl-pyridines between S-pyI, F-pyI and W-pyI, which also have a certain degree of influence on the values of TPA cross-sections. Therefore, the acceptor strength and flatness of a “fluorenone” central aromatic core should be higher than those of “dibenzothiophene,” “fluorenone,” or “carbazole,” giving W-pyI stronger electron-withdrawing capacity and better ICT efficiency in  $\pi$ -conjugated delocalized systems.

### DNA fluorescence switching

To investigate the DNA-targeting abilities of W-pyI, S-pyI, and F-pyI, DNA fluorescence switching experiments were performed in Tris-HCl buffer solution. The absorption, one- and two-photon fluorescence “turn-on” experiments performed in the presence of ct-DNA are shown in Fig. 5. Based on the trend and degree of change in the spectra, we can determine the mode of binding between these probes and double-stranded ct-DNA, and also judge the influence on probe performance and mechanism of central conjugated bridges with different aromatic structures [33]. As shown in Fig. 5, absorbance all gradually decreased along with slight red shifts of absorption spectrum as the DNA concentration increased to saturation, displaying an obvious hypochromic trend (Fig.5 I). In contrast, dramatic enhancements in both one- and two-photon fluorescence intensity were observed as the concentration ratio approached saturation ( $[\text{DNA}]:[\text{probe}] > 140:1$ ) for W-pyI, S-pyI, and F-pyI, which showed an apparent hyperchromic effect (Fig.5 II and III). Based on previous research, these V-shaped conjugated probes may show intercalative binding or minor groove binding to double-stranded DNA. Furthermore, as the DNA concentration increased to saturation, 58-fold, 30-fold, and 25-fold enhancements in fluorescence quantum yields were observed for W-pyI, S-pyI, and F-pyI, respectively. A 350–450% increase in TPA cross-section was also observed for these new probes. The fluorescence enhancement could be explained in the following way: when these probes recognize nucleobases with their terminal pyridinium salt units, rotation of their pendant vinylpyridine arms is restricted by the phosphate backbones of the DNA molecules, greatly reducing the nonradiative decay [34,35]. We also referred to the related

performance values of biscarbazolymethane-based pyridinium salts bonding with DNA in Tris-HCl buffer solutions, which showed an approximately 30-fold fluorescence enhancement and 3-fold enhancement of the TPA cross-section at saturation [10]. Moreover, the indole-based mono-cationic probes INR1 and INR2 in the presence of DNA in buffer solutions exhibited approximately 2.5-fold and 2.14-fold in fluorescence quantum yields, respectively [12]. Thus, W-pyI with a central “fluorenone” conjugated aromatic core showed stronger DNA fluorescence switching capacity than that with a “dibenzothiophene,” “dibenzofuran,” “carbazole” or “indole” core, which meant that the central  $\pi$ -conjugated bridge played a leading part in the fluorescence “turn-on” effect. Meanwhile, in addition to the action of the conjugated aromatic core, the different linkage position of the central core and two vinyl-pyridines for these V-shaped fluorescent probes had some impacts on the DNA fluorescence switching to a certain extent as well. At present, the mechanism by which the central  $\pi$ -conjugated bridges influence the fluorescence “turn-on” effect remains unclear. According to a previous study, this phenomenon may be attributed to the following reason [23]: when these probes bind to double-stranded DNA, they gradually interact with the nucleobases, and the charge spacing of the “fluorenone” aromatic core is more compatible with the inter-phosphate distance of the DNA molecules. Thus, compared with S-pyI, F-pyI, and the pyridine cation salts with “carbazole” or “indole” cores, W-pyI had a better fluorescence effect owing to its intercalative or minor groove binding mode.

### Confocal fluorescence imaging

To explore the application of the two-photon fluorescent probes to cellular imaging, two-photon excited fluorescence imaging of W-pyI, S-pyI, and F-pyI in 3T3 cells was performed using femtosecond laser excitation at 800 nm, as shown in Fig.6. Cells stained with W-pyI (Fig.6 I), S-pyI (Fig.6 II), and F-pyI (Fig.6 III) emitted bright green and blue fluorescence, respectively. The brightness met the requirements for monitoring and tracking in two-photon fluorescence biological imaging. In addition, to investigate the difference between one-photon and two-photon imaging effects, one- and two-photon fluorescence imaging of W-pyI, S-pyI, and F-pyI in 3T3 cells was performed with an excitation wavelength of 405 nm and 800 nm, as exhibited in Fig.7. Because the main emission bands for one- and two-photon fluorescence were in the same range, to facilitate distinguishing the fluorescence strength in the images, the two-photon fluorescence color of W-pyI, S-pyI, and F-pyI was set to red using built-in software. As shown in Fig.7, obvious yellow (Fig.7 Id, IId) and pink (Fig.7 IIId) fluorescence were observed in the merged images, which indicated strong similarity between the brightness of one- and two-photon fluorescence imaging. However, due to relatively lower levels of background noise produced by small Rayleigh scattering

in the two-photon absorption process, two-photon fluorescence imaging possessed higher resolution and a better signal-to-noise ratio [14].

### **Nuclear localization and counterstaining experiments**

To investigate the nuclear targeting abilities of the probes, co-localization studies were performed using W-pyI, S-pyI, or F-pyI and Hoechst 33342 in 3T3 cells. Hoechst 33342 is a commercial nuclear staining agent, and served as a baseline for judging the accuracy of nuclear localization of W-pyI, S-pyI, and F-pyI by measuring the degree of co-localization. Notably, F-pyI and Hoechst 33342 both emit blue fluorescence, while the optimal one-photon excitation wavelength of Hoechst 33342 are located near 350 nm in the bioenvironment, and there is extremely weak fluorescence emission at 405 nm for Hoechst 33342 in cells imaging. Thus, the color of F-pyI fluorescence could be set to red under laser excitation at 405 nm for ease of observation and discrimination. As shown in Fig.8, staining with W-pyI, S-pyI, or F-pyI and Hoechst 33342 showed a high degree of fluorescence overlapping in the nucleus (Fig.8 Ic, IIc, and IIIc). Using built-in software, the mean co-localization coefficients between W-pyI, S-pyI, or F-pyI and Hoechst 33342 were determined to be 0.91, 0.92 and 0.89, respectively, confirming that W-pyI, S-pyI, and F-pyI possess accurate nuclear localization.

To investigate counterstaining compatibility for multicolor labeling in the cellular microenvironment, a counterstaining experiment employing W-pyI, S-pyI or F-pyI co-stained with MTR were performed in 3T3 cells. As shown in Fig.9, red fluorescence was emitted from the peripheral cytoplasmic regions, and the central nuclear positions, targeted by W-pyI, S-pyI, and F-pyI, produced bright green (Fig.9 a and b) and blue (Fig.9 c) fluorescence, respectively. Thus, W-pyI, S-pyI, and F-pyI show good counterstaining compatibility with MTR. Moreover, the probes appear to have entered the nuclear pores smoothly, showing their water solubility and membrane permeability in the cellular microenvironment. Hence, they could be applied in the study of biological imaging, which referred to physiological activity of the nuclei to complete multicolor targeting.

### **Photostability studies**

Photostability mainly refers to resistance of a fluorescent probe to laser radiation aging in biological fluorescence imaging. Under continuous excitation with a high-power laser, the molecular structure will be destroyed to a certain extent, causing the fluorescence intensity to decrease with time, resulting in photobleaching. Therefore, the design of the molecular structure is a key factor in photostability [36]. Here, the time-dependent two-photon fluorescence intensity of W-pyI, S-pyI, and

F-pyI was tested under continuous excitation with a femtosecond laser operating at 800 nm in 3T3 cells. Using the built-in software, the confocal fluorescence microscope captured an image every 30 seconds. As shown in Fig.10–Fig.13, under excitation at the same power, the fluorescence intensity of each probe gradually decreased until it was almostly quenched. However, the duration of fluorescence emission varied greatly between W-pyI, S-pyI, and F-pyI: 3000 s, 1800 s and 540 s, respectively. Furthermore, the fluorescence attenuation efficiency of W-pyI, S-pyI, and F-pyI over the whole fluorescence decay process was 0.026%/s, 0.033%/s, and 0.081%/s, and the fluorescence attenuation amplitude ( $\delta$ ) was approximately 7.1%, 9.7%, and 33% in the first 300 s. Compared to some previously reported two-photon fluorescent labels, for example, carbazole-based pyridine cation salts [11],  $\delta = 10\%$  and  $20\%$ ; indole-based mono-cationic derivatives [12],  $\delta = 8\%$  and  $28\%$ ; dinuclear Ru(II) polypyridyl complex [14],  $\delta = 38\%$ , our W-pyI with the “fluorenone” central  $\pi$ -conjugated bridge showed relatively better photostability than those above probes in two-photon fluorescence cellular imaging. This was consistent with the previous results for TPA cross-sections and the DNA fluorescence switching effect. This result can be attributed to the following two factors [37-40]: from the perspective of molecular structure, there was a high degree of matching between the lattice structure or charge spacing of the fluorenone aromatic core and the DNA phosphate backbone, resulting in easier binding of the AT-rich regions of the minor grooves in the DNA; from the perspective of electron energy level transition, fluorenone may show stronger electron-withdrawing capacity due to the presence of oxygen atom in the carbonyl group, increasing the ICT efficiency between the central fluorenone bridge and the terminal electron-donating pyridinium group inside the  $\pi$ -conjugated delocalized system. Therefore, W-pyI exhibited better photostability in these homogeneous molecular structures with different central  $\pi$ -conjugated bridges. Furthermore, these results indicate that, in the design of future two-photon fluorescence probes, the  $\pi$ -conjugated core should be connected with atoms or groups with high strength, good flatness, and strong electron-withdrawing properties, permitting stable electron transfer from the terminal electron donors.

## Conclusions

In conclusion, a series of novel two-photon mono-cationic pyridinium probes with different central  $\pi$ -conjugated aromatic cores, fluorenone, dibenzothiophene, and dibenzofuran, were prepared. The one- and two photophysical properties showed that W-pyI has the optimal electron withdrawing capacity and ICT efficiency inside the molecular  $\pi$ -conjugated delocalized system, with a fluorescence quantum yield of 0.401 and TPA cross-sections of 681 GM in DMF. In the DNA fluorescence switching

experiment, W-pyI showed a 58-fold fluorescence enhancement and 450% TPA cross-section increasement, indicating that it had higher fluorescence “turn-on” effect than the S-pyI, F-pyI, or carbazole-based fluorescent probes. Under a confocal microscope, with excitation at wavelengths of 405 nm and 800 nm, one- and two-photon fluorescence imaging of all of these mono-cationic pyridinium probes was clear. The mean co-localization coefficient of 0.89–0.92 between these probes and Hoechst 33342 in 3T3 cells indicated that W-pyI, S-pyI, and F-pyI all possess accurate nuclear targeting abilities. The counterstain test showed that all three probes show good counterstaining compatibility with MTR, as well as membrane permeability in the cellular microenvironment. Finally, the fluorescence duration of 3000 s, the fluorescence attenuation efficiency of 0.026%/s, and the fluorescence attenuation amplitude of 7.1% within 300 s illustrated that W-pyI shows better photostability than the S-pyI, F-pyI, carbazole-based, and indole-based probes from the perspective of molecular structure and electron energy level transition. Therefore, in addition to having strong electron-donating abilities and sensitive recognition units, the excellent electron-withdrawing capacity, good flatness, suitable biocompatibility and effective binding mechanism of the central  $\pi$ -conjugated bridges are key features in the design of two-photon fluorescent probes for nuclear imaging.

### Acknowledgements

This research was supported in part by the National Natural Science Foundation of China (Grant Nos. 61137002, 61178059 and 51172253).

### Notes and references

- [1] U. K. Tirlapur and K. Konig, *Nature*, 2002, **418**, 290.
- [2] A. W. Zhu, C. Q. Ding and Y. Tian, *Sci. Rep.*, 2013, **3**, 2933.
- [3] D. R. Larson, W. R. Zipfel, R. M. Williams, S. W. Clark, M. P. Bruchez, F. W. Wise and W. W. Webb, *Science*, 2003, **300**, 1434.
- [4] F. Helmchen and W. Denk, *Nat. Methods*, 2005, **2**, 932.
- [5] L. Li, C. W. Zhang, G. Y. J. Chen, B. W. Zhu, C. Chai, Q. H. Xu, E. K. Tan, Q. Zhu, K. L. Lim and S. Q. Yao, *Nat. Commun.*, 2014, **5**, 3276.
- [6] S. A. Ranjan, K. D. Eun, K. H. Myung and C. B. Rae, *Inorg. Chem.*, 2013, **53**, 1794.
- [7] P. Ning, J. Jang, L. Li, S. Wang, H. Yu, Y. Feng, M. Zhu, B. Zhang, H. Yin, Q. Guo

- and X. Meng, *Biosens. Bioelectron.*, 2015, **77**, 921.
- [8] Y. M. Ho, N. P. B. Au, K. L. Wong, C. T. L. Chan, W. M. Kowk, G. L. Law, K. K. Tang, W. Y. Wong, C. H. E. Ma and M. H. W. Lam, *Chem. Commun.*, 2014, **50**, 4161.
- [9] Y. He, Z. Wang, Y. Wang, L. Wei, X. Li, J. Yang, G. Shi and Y. Zhang, *Chin. Opt. Lett.*, 2015, **13**, 111702.
- [10] Y. C. Zheng, M. L. Zheng, S. Chen, Z. S. Zhao and X. M. Duan, *J. Mater. Chem. B*, 2014, **2**, 2301.
- [11] F. Miao, W. J. Zhang, Y. M. Sun, R. Y. Zhang, Y. Liu, F. Q. Guo, G. F. Song, M. G. Tian and X. Q. Yu, *Biosens. Bioelectron.*, 2014, **55**, 423.
- [12] Y. Liu, W. J. Zhang, Y. M. Sun, G. F. Song, F. Miao, F. Q. Guo, M. G. Tian, X. Q. Yu and J. Z. Sun, *Dyes. Pigments.*, 2014, **103**, 191.
- [13] J. J. Wang, Y. M. Sun, W. J. Zhang, Y. Liu, X. Q. Yu and N. Zhao, *Talanta*, 2014, **129**, 241.
- [14] W. C. Xu, J. R. Zuo, L. L. Wang, L. N. Ji and H. Chao, *Chem. Commun.*, 2014, **50**, 2123.
- [15] K. Sreenath, Z. Yuan, J. R. Allen, M. W. Davidson and L. Zhu, *Chem-Eur. J.*, 2015, **21**, 867.
- [16] A. R. Morales, K. D. Belfield, J. M. Hales, E. W. Van Stryland and D. J. Hagan, *Chem. Mater.*, 2006, **18**, 4972.
- [17] X. D. Zhang, H. X. Wang, H. Wang, Q. Zhang, J. F. Xie, Y. P. Tian, J. Wang and Y. Xie, *Adv. Mater.*, 2014, **26**, 4438.
- [18] H. Zhang, J. L. Fan, K. Wang, J. Li, C. X. Wang, Y. M. Nie, T. Jian, H. Y. Mu, X. J. Peng and K. Jiang, *Anal. Chem.*, 2014, **86**, 9131.
- [19] H. Y. Ahn, S. Yao, X. Wang and K. D. Belfield, *ACS Appl. Mater. Inter.*, 2012, **4**, 2847.
- [20] W. Zhang, X. Wang, P. Li, F. Huang, H. Wang, W. Zhang and B. Tang, *Chem. Commun.*, 2015, **51**, 9710.
- [21] W. V. Moreshead, O. V. Przhonska, M. V. Bondar, A. D. Kachkovski, I. H. Nayyar, A. E. Masunov, A. W. Woodward and K. D. Belfield, *J. Phys. Chem. C*, 2013, **117**, 23133.
- [22] A. R. Morales, A. Frazer, A. W. Woodward, H. Yang, A. White, A. Fonari, P. Tongwa, Tatiana, Timofeeva and K. D. Belfield, *J. Org. Chem.*, 2013, **78**, 1014.

- [23] D. R. G. Pitter, J. Wiggenius, A. S. Brown, J. D. Baker, F. Westerlund and J. N. Wilson, *Org. Lett.*, 2013, **15**, 1330.
- [24] E. A. Mensah, W. G. Gonzalez, D. R. Busse, B. Captain, J. Miksovská and J. N. Wilson, *J. Phys. Chem. A*, 2012, **116**, 8671.
- [25] J. Dhuguru, C. Gheewala, N. S. S. Kumar and J. N. Wilson, *Org. Lett.*, 2011, **13**, 4188.
- [26] C. Xu and W. W. Webb, *J. Opt. Soc. Am. B*, 1996, **13**, 481.
- [27] R. Wolleschensky, T. Feurer, R. Sauerbrey and U. Simon, *Appl. Phys. B*, 1998, **67**, 87.
- [28] H. P. Zhou, D. M. Li, J. Z. Zhang, Y. M. Zhu, J. Y. Wu, Z. J. Hu, J. X. Yang, G. B. Xu, Y. P. Tian and Y. Xie, *Chem. Phys.*, 2006, **322**, 459.
- [29] X. J. Feng, P. L. Wu, F. Bolze, H. W. C. Leung, K. F. Li, N. K. Mak, D. W. J. Kwong, J. F. Nicoud, K. W. Cheah and M. S. Wong, *Org. Lett.*, 2010, **12**, 2194.
- [30] Y. H. Zhang, J. J. Wang, P. F. Jia, X. Q. Yu, H. Liu, X. Liu, N. Zhao and B. B. Huang, *Org. Biomol. Chem.*, 2010, **8**, 4582.
- [31] F. Miao, G. F. Song, Y. M. Song, Y. Liu, F. Q. Guo, W. J. Zhang, M. G. Tian and X. Q. Yu, *Biosens. Bioelectron.*, 2013, **50**, 42.
- [32] J. Kawamata, M. Akiba, T. Tani, A. Harada and Y. Inagaki, *Chem. Lett.*, 2004, **33**, 448.
- [33] L. T. Jin, S. Y. Hwang, G. S. Yoo and J. K. Choi, *Electrophoresis*, 2004, **25**, 2429.
- [34] C. Chang, J. F. Chu, H. Kuo, C. C. Kang, S. Lin and T. Chang, *J. Luminesc.*, 2006, **119**, 84.
- [35] H. Malak, F. N. Castellano, I. Gryczynski and J. R. Lakowicz, *Biophys. Chem.*, 1997, **67**, 35.
- [36] J. E. A. Otterstedt, *J. Phys. Chem.*, 1973, **58**, 5718.
- [37] S. Neidle, *Nat. Prod. Rep.*, 2001, **18**, 291.
- [38] C. Bailly and J. B. Chaires, *Bioconj. Chem.*, 1998, **9**, 513.
- [39] F. A. Tanious, P. D. Bailly, C. R. R. Tidwell, W. D. Wilson and D. Y. Ding, *Biochemistry*, 2000, **39**, 12091.

[40] J. Aymami, C. M. Nunn and S. Neidle, *Nucleic Acids Res.*, 1999, **27**, 2691.

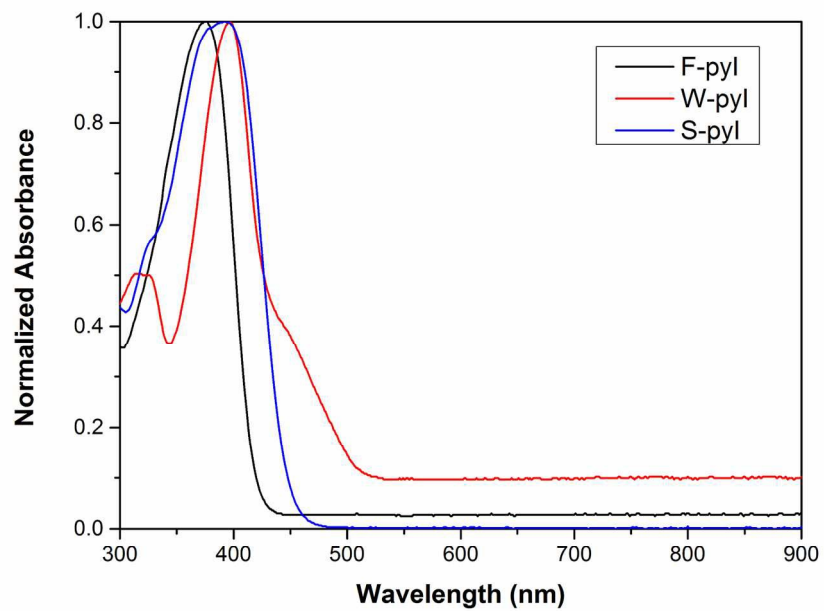


Fig.1 Normalized absorption spectra of W-pyI, S-pyI, and F-pyI in DMF,  $[W\text{-pyI}] = [S\text{-pyI}] = [F\text{-pyI}] = 10^{-5}$  M.

148x104mm (300 x 300 DPI)

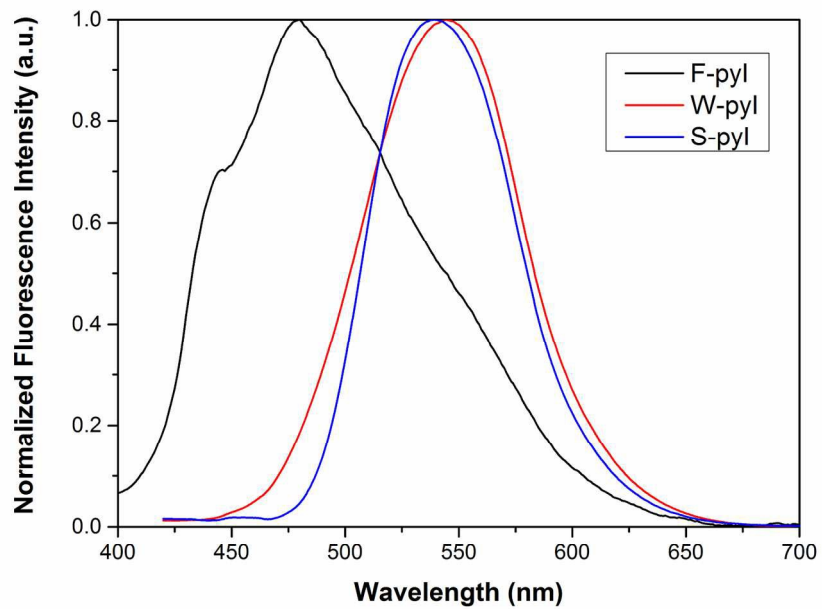


Fig.2 Normalized one-photon fluorescence spectra of W-pyI, S-pyI, and F-pyI in DMF,  $[W\text{-pyI}] = [S\text{-pyI}] = [F\text{-pyI}] = 10^{-5}$  M.

148x104mm (300 x 300 DPI)

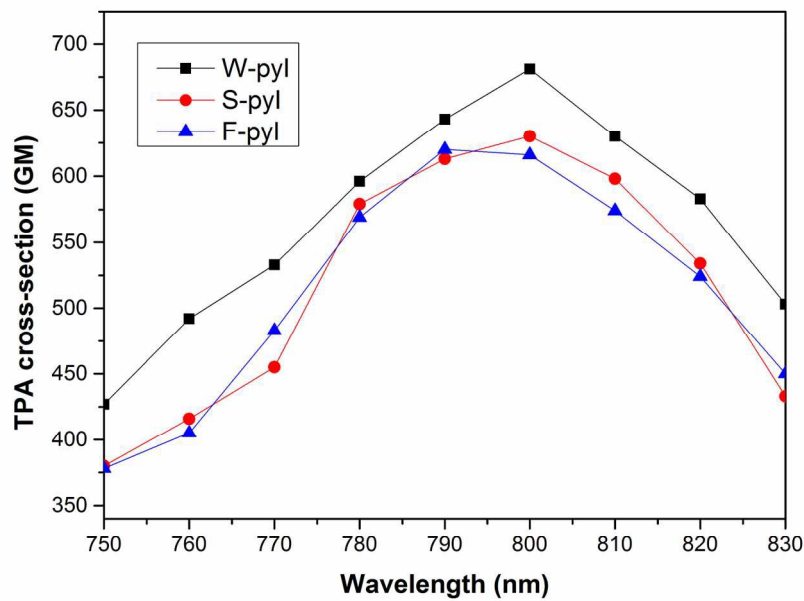


Fig.3 Two-photon absorption cross-sections of W-pyI, S-pyI, and F-pyI in the excitation wavelength ranging from 750 to 830 nm in DMF,  $[W-pyI]=[S-pyI]=[F-pyI]=10^{-4}$  M.

148x104mm (300 x 300 DPI)

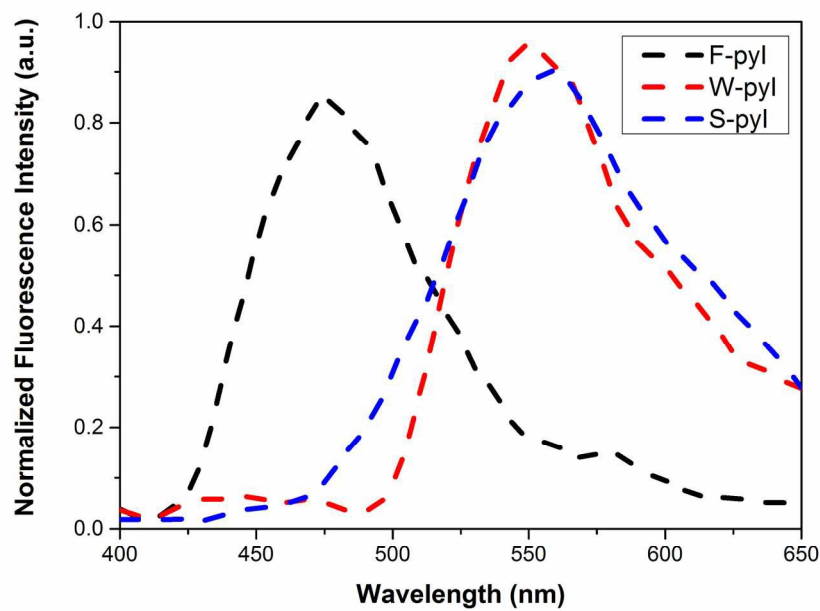


Fig.4 Two-photon fluorescence spectra of W-pyI, S-pyI, and F-pyI at excitation wavelength of 800 nm in DMF,  $[W\text{-pyI}] = [S\text{-pyI}] = [F\text{-pyI}] = 10^{-4}$  M.

148x104mm (300 x 300 DPI)

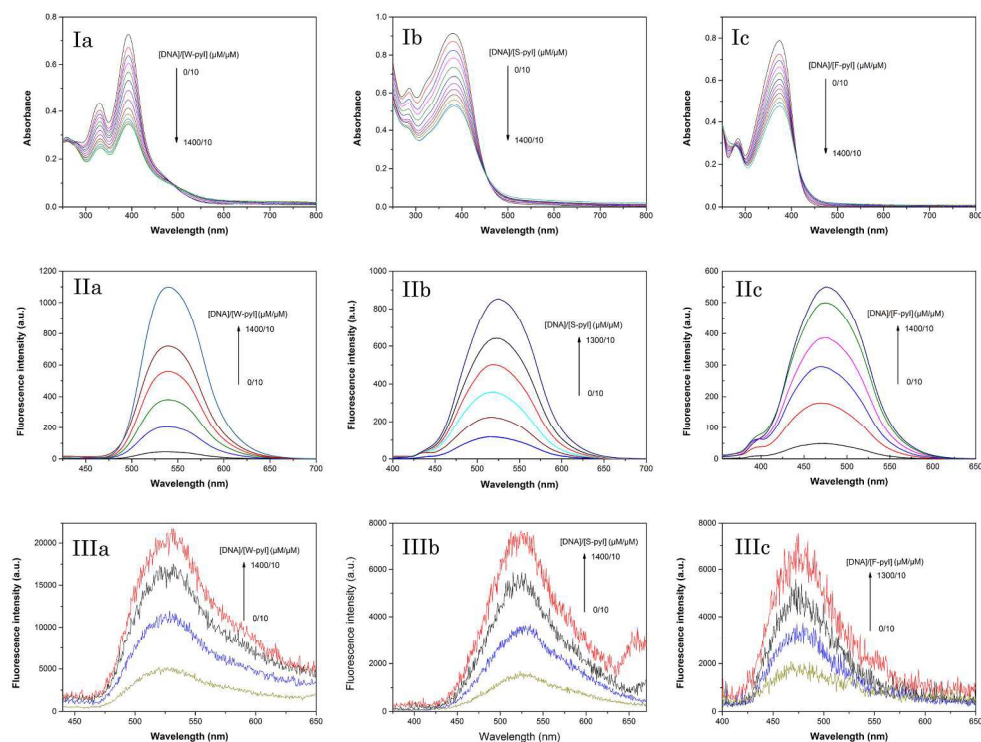


Fig.5 Absorption (I), one-photon (II) and two-photon fluorescence (III) spectra of W-pyI (a), S-pyI (b), and F-pyI (c) as a function of different DNA concentration in Tris-HCl buffer solutions.  $[W\text{-pyI}] = [S\text{-pyI}] = [F\text{-pyI}] = 10^{-5}$  M,  $[DNA] = 0 - 1.4 \times 10^{-3}$  M. The arrows represent the increasing or decreasing trends.

200x150mm (300 x 300 DPI)

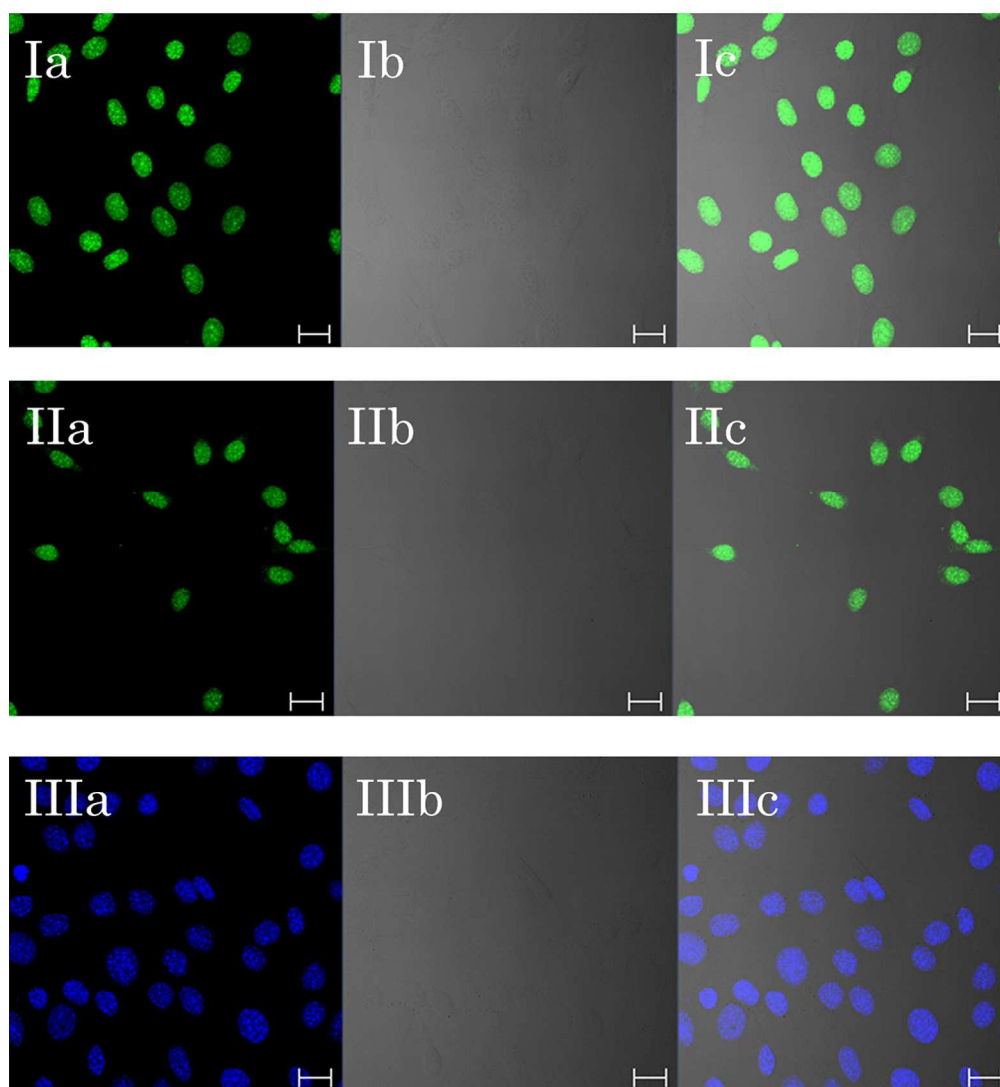


Fig.6 Two-photon confocal fluorescence imaging of 3T3 cells stained with W-pyI (I, 0.3  $\mu\text{M}$ ), S-pyI (II, 0.3  $\mu\text{M}$ ) and F-pyI (III, 0.3  $\mu\text{M}$ ) for 15 min. I and II:  $\lambda_{\text{em}} = 525\text{--}575\text{ nm}$ ; III:  $\lambda_{\text{em}} = 430\text{--}490\text{ nm}$ ; (a) Two-photon fluorescence images; (b) DIC pictures; (c) Overlay images of a and b.  $\lambda_{\text{exc}} = 800\text{ nm}$ , Bar = 20  $\mu\text{m}$ .

104x115mm (300 x 300 DPI)

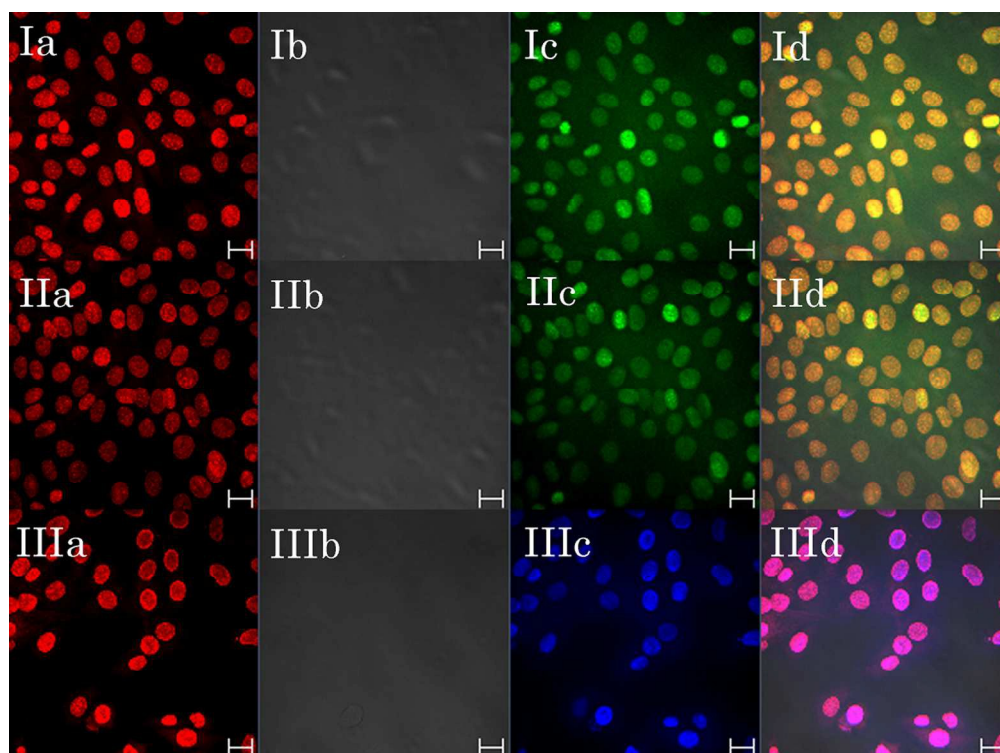


Fig.7 One- and two-photon confocal fluorescence images of 3T3 cells stained with W-pyI (I, 0.3  $\mu\text{M}$ ), S-pyI (II, 0.3  $\mu\text{M}$ ) and F-pyI (III, 0.3  $\mu\text{M}$ ) for 15 min. (a) Two-photon fluorescence images,  $\lambda_{\text{ex}} = 800 \text{ nm}$ ; (b) DIC pictures; (c) One-photon fluorescence images,  $\lambda_{\text{ex}} = 405 \text{ nm}$ ; (d) Overlay images of a and c. I and II:  $\lambda_{\text{em}} = 525\text{--}575 \text{ nm}$ , III:  $\lambda_{\text{em}} = 430\text{--}490 \text{ nm}$ . Bar = 20  $\mu\text{m}$ .

106x80mm (300 x 300 DPI)

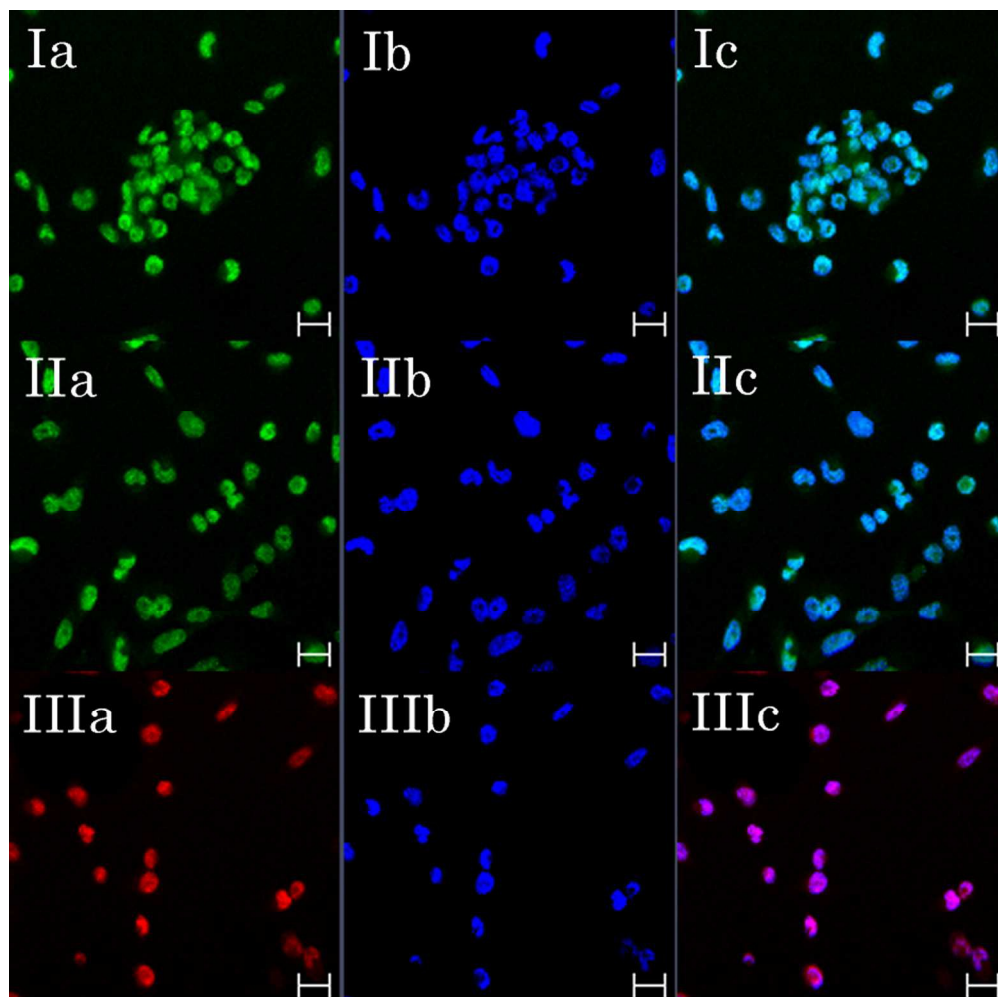


Fig.8 Confocal fluorescent images of 3T3 cells double-stained with W-pyI (Ia, 0.3  $\mu$ M), S-pyI (IIa, 0.3  $\mu$ M) or F-pyI (IIIa, 0.3  $\mu$ M) and Hoechst 33342 (b, 0.3  $\mu$ M) for 15 min. (a) images of W-pyI (I), S-pyI (II) and F-pyI (III),  $\lambda_{\text{ex}} = 405$  nm, I and II:  $\lambda_{\text{em}} = 525\text{--}575$  nm; III:  $\lambda_{\text{em}} = 430\text{--}490$  nm; (b) images of Hoechst 33342,  $\lambda_{\text{ex}} = 330\text{--}380$  nm, and  $\lambda_{\text{em}} = 430\text{--}490$  nm; (c) overlay images of a and b. Bar = 20  $\mu$ m.

80x80mm (300 x 300 DPI)

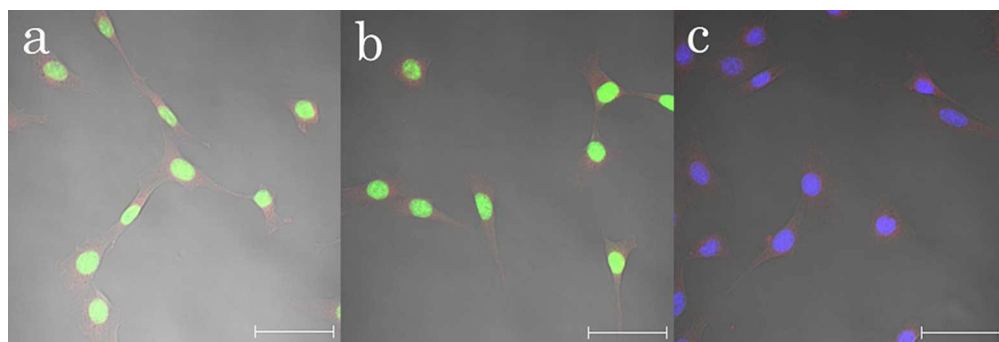


Fig.9 Confocal fluorescence images of 3T3 cells co-stained with W-pyI (a, 0.3  $\mu$ M), S-pyI (b, 0.3  $\mu$ M), or F-pyI (c, 0.3  $\mu$ M) and MTR (a–c, 0.3  $\mu$ M) for 15 min. For W-pyI and S-pyI,  $\lambda_{\text{ex}}$  = 405 nm, and  $\lambda_{\text{em}}$  = 525–575 nm. For F-pyI,  $\lambda_{\text{ex}}$  = 330–380 nm, and  $\lambda_{\text{em}}$  = 430–490 nm. For MTR,  $\lambda_{\text{ex}}$  = 575 nm, and  $\lambda_{\text{em}}$  = 580–650 nm. Bar = 20  $\mu$ m.

78x26mm (300 x 300 DPI)

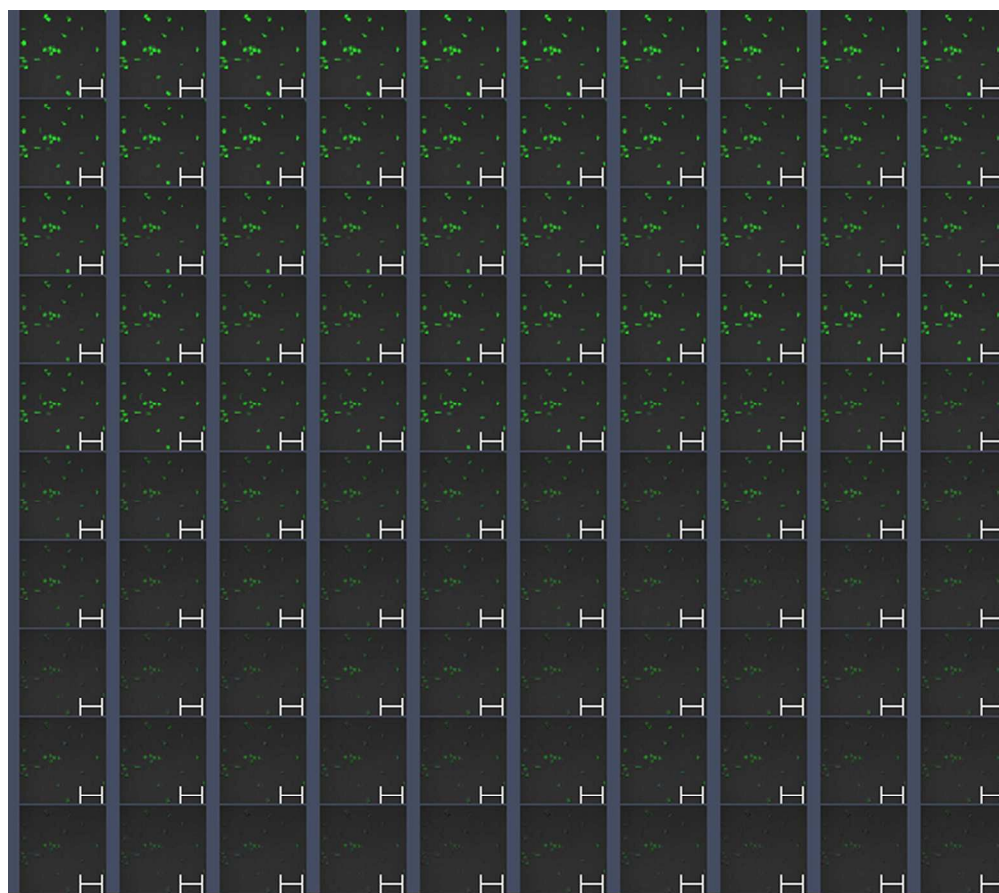


Fig.10 Time-dependent two-photon fluorescence imaging of 3T3 cells stained with W-pyI (0.3  $\mu\text{M}$ ) for 15 min,  $\lambda_{\text{ex}}$  = 800 nm, and  $\lambda_{\text{em}}$  = 525–575 nm. Bar = 50  $\mu\text{m}$ .

105x93mm (300 x 300 DPI)

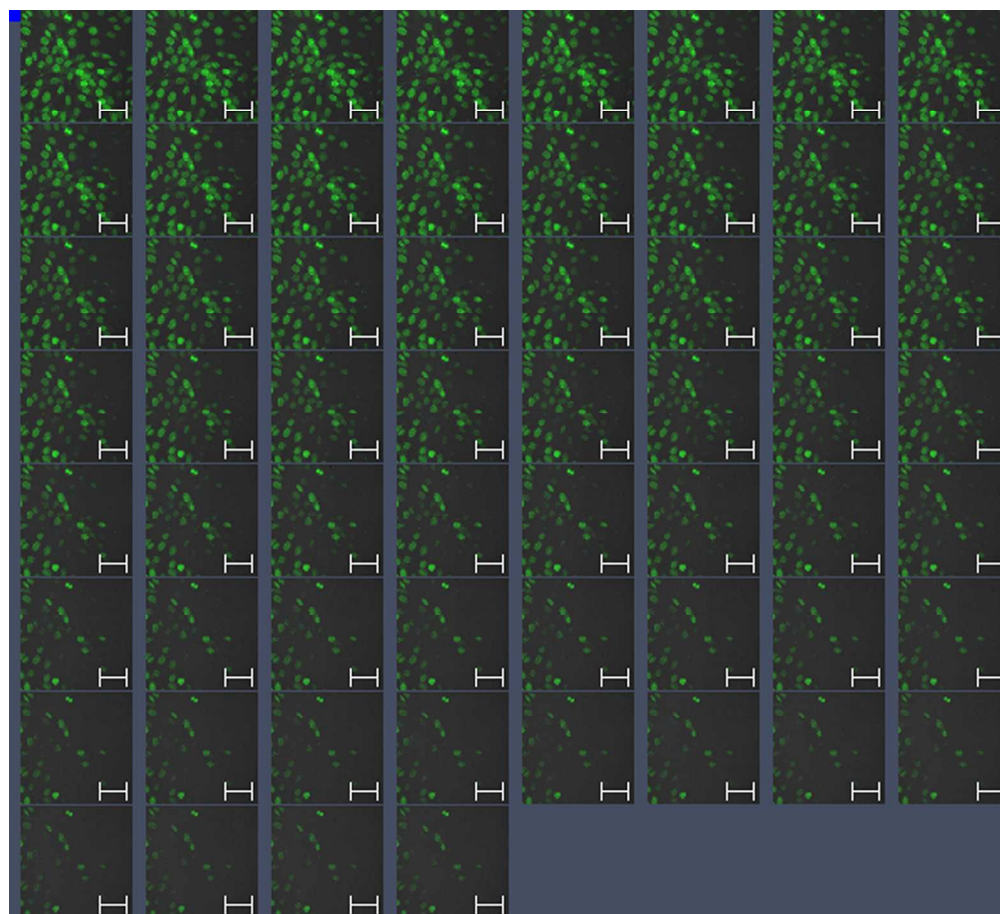


Fig.11 Time-dependent two-photon fluorescence imaging of 3T3 cells stained with S-pyI (0.3  $\mu\text{M}$ ) for 15 min,  $\lambda_{\text{ex}}$  = 800 nm, and  $\lambda_{\text{em}}$  = 525–575 nm. Bar = 50  $\mu\text{m}$ .

105x95mm (300 x 300 DPI)

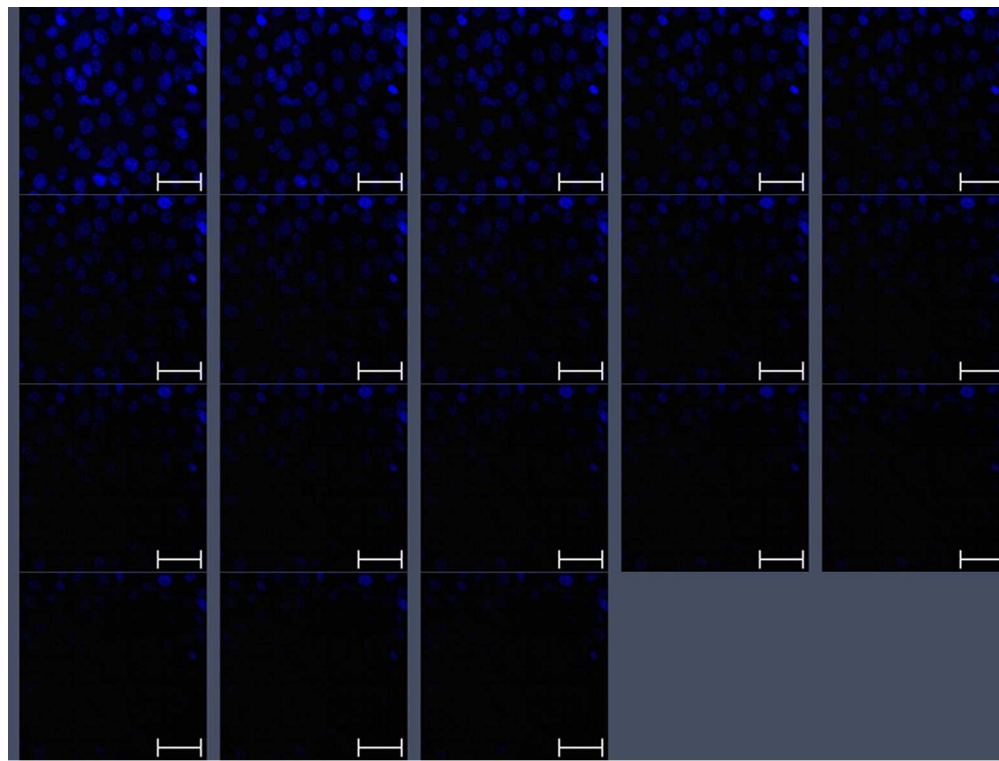


Fig.12 Time-dependent two-photon fluorescence imaging of 3T3 cells stained with F-pyI (0.3  $\mu\text{M}$ ) for 15 min,  $\lambda_{\text{ex}} = 330\text{--}380\text{ nm}$ , and  $\lambda_{\text{em}} = 430\text{--}490\text{ nm}$ . Bar = 50  $\mu\text{m}$ .

106x80mm (300 x 300 DPI)

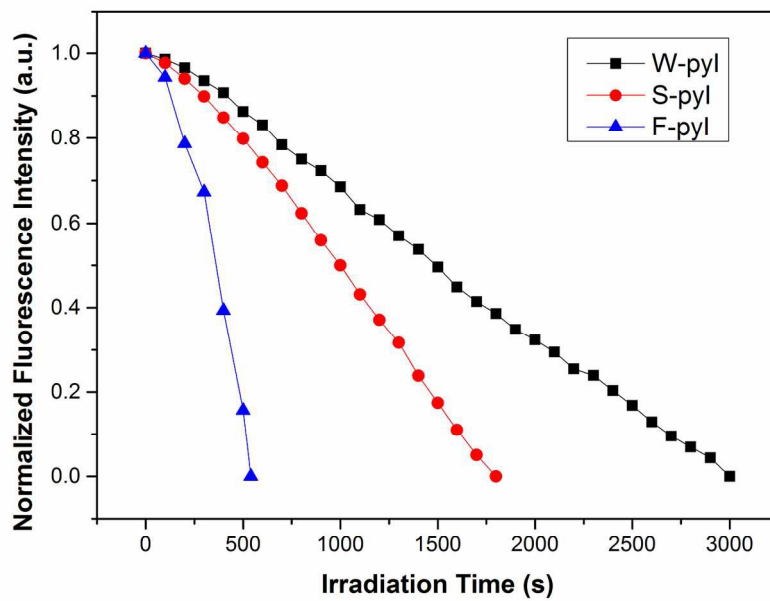
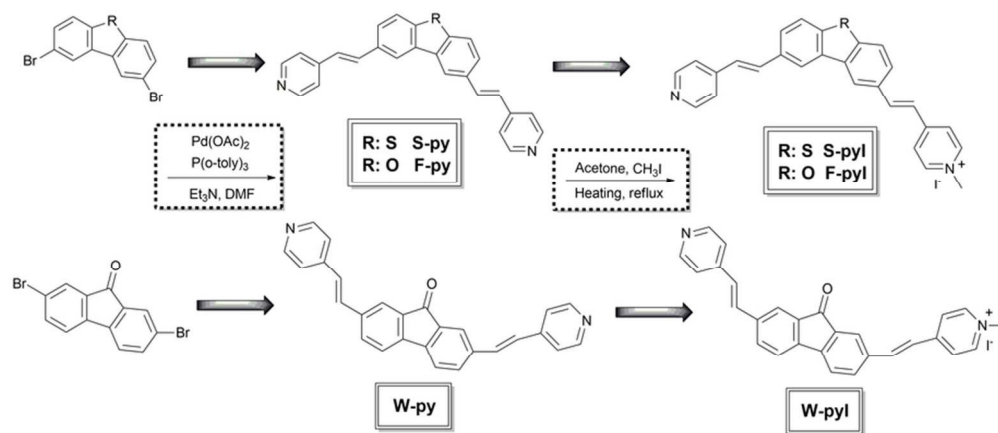


Fig.13 Normalized two-photon fluorescence intensity attenuation of W-pyI, S-pyI, and F-pyI as time variation under continuous irradiation.

148x104mm (300 x 300 DPI)



Scheme 1. Synthesis of mono-cationic fluorescent probes

77x33mm (300 x 300 DPI)

## Graphical Abstract

A series of novel pyridine mono-cationic two-photon fluorescent probes based on different central  $\pi$ -conjugated bridges, fluorenone (W-pyI), dibenzothiophene (S-pyI), and dibenzofuran (F-pyI), were prepared and studied. Under one-photon excitation in N,N-dimethylformamide solution, W-pyI, S-pyI, and F-pyI displayed fluorescence quantum yields of 0.401, 0.425, and 0.09, respectively. The two-photon fluorescence performance indicated that these probes possessed large two-photon absorption cross-sections of 681 GM (W-pyI), 630 GM (S-pyI), and 620 GM (F-pyI) at 800-nm femtosecond laser excitation. The luminance “turn-on” effect of W-pyI, S-pyI, and F-pyI bonding with calf thymus DNA in Tris-HCl buffer solutions displayed 58-fold, 30-fold, and 25-fold fluorescence quantum yield increments, respectively, and 350–450% two-photon absorption cross-section enhancement. The confocal fluorescence imaging showed clear one- and two-photon fluorescence imaging. The mean co-localization coefficients between these probes and Hoechst 33342 in 3T3 cells ranged from 0.89–0.92, indicating that they showed excellent nuclear targeting abilities. The counterstaining experiments exhibited these probes possessed good counterstaining compatibility and membrane permeability in the application of multicolor targeting. The time-dependent fluorescence intensity test under continuous femtosecond laser irradiation showed that W-pyI possessed a longer observation time (3000 seconds) and a lower fluorescence attenuation amplitude (7.1%) in the first 300 seconds than S-pyI, F-pyI and other previously reported pyridinium derivatives, demonstrating that the central  $\pi$ -conjugated bridge “fluorenone” played a key role in improving photostability during probe designing for two-photon bioimaging applications.

